Temperature-Independent Rate of Electron-Transfer between a Cobalt(II) and a Ruthenium(III) of Doublet Electronic Configuration

Hiroaki Torieda, Akio Yoshimura,* Koichi Nozaki, Satomi Sakai, and Takeshi Ohno*

Department of Chemistry, Graduate School of Science, Osaka University, 1-16 Machikaneyama, Toyonaka, Osaka 560-0043, Japan

Received: May 21, 2002; In Final Form: August 12, 2002

A study of laser kinetic spectroscopy on $[Ru^{II}(tpy)(BL)Co^{III}(tpy)]^{5+}$ (BL: 1,4-bis[2,2′:6′,2″-terpyridine-4′-yl]benzene (btbz) and 6′,6″-bis(2-pyridyl)- 2,2′:4′,4″:2″,2‴-quarter-pyridine (bpqp)) revealed rise-and-decay of a triplet Ru-to-ligand charge-transfer state, ^{3}CT(Ru), and an electron-transfer product of $[(tpy)Ru^{III}(BL)Co^{II}(tpy)]^{5+}$. ^{3}CT(Ru) underwent electron-transfer with a rate constant of 0.3×10^{12} and 1×10^{12} s^{-1} to produce $[(tpy)Ru^{III}(BL)Co^{II}(tpy)]^{5+}$ with a doublet electronic configuration $d_\pi{}^6d_{\sigma^*}$ of cobalt(II). The return electron transfer (RET) of $[Ru^{III}(tpy)(BL)Co^{II}(tpy)]^{5+}$ (BL:btbz and bpqp) in acetonitrile occurred with a rate constant of 1×10^{10} and 6×10^{10} s^{-1} at 298 K, respectively, which are much faster than intramolecular RET of $[(bpy)_2Ru(BL)Co(bpy)_2]^{5+}$ from cobalt(II) with a quartet electronic configuration of $d_\pi{}^5d_{\sigma^*}{}^2$. The magnitude of reorganization energy (0.95 ± 0.15 eV) and electronic coupling matrix element (0.8 and 2 meV) are evaluated from the independence of RET rate on the temperature by using a small entropy change of RET. The small intramolecular reorganization energy (0−0.3 eV) for ^{2}Co(II)/^{1}Co(III) redox process of $[(tpy)Ru^{II}(BL)Co^{III}(tpy)]^{5+}$ (BL: btbz and bpqp) are responsible for the fast RET. The magnitude of the intramolecular reorganization energy is in agreement with those (0.27−0.29 eV) calculated by using a density functional theory.

Introduction

Elementary electron-transfer processes of donor−acceptor compounds in solution have been studied in order to elucidate magnitude of electronic transmission coefficient κ_{et} and nuclear factor κ_n

$$k_{et} = \nu_n \kappa_{et} \kappa_n \tag{1}$$

where ν_n is effective vibrational frequency. When intermolecular transfer of electron is accompanied by a large displacement of nucleus, not only high-frequency modes of vibration but also medium- and low-frequency modes can be involved in electron-transfer processes. Hence, the nuclear factor plays a crucial and complex role in the electron transfer. As for nonradiative processes accompanied by excitation of low- and medium-frequency vibrations of initial and final states,[1,2] a simple energy gap law is not applicable any more. An important role of nuclear displacement as well as electron transmission in electron transfer has been pointed out for electron-transfer processes of Co(II) compounds

$$^{4,2}\text{Co(II)} \rightarrow {}^1\text{Co(III)} + \text{e} \tag{2}$$

where the metal−ligand bond lengths are largely changed by 10−45 pm.[3−8] Thermal excitation of the vibration modes of reactant and solvation mode precedes electron transfer in the normal region so that the electron transfer rate is simply dependent on temperature. Meanwhile, formation of vibrational excited states of the product in the inverted region makes the electron-transfer rate not to decrease at lower temperatures because of the tunneling effect if the nuclear displacement is fairly large.

Classical and quantum chemical calculations[9−12] have been examined to assess the nuclear factor and the electronic transmission coefficient of electron exchange reaction and intramolecular electron transfer in the normal region. A classical nuclear factor can be written

$$\kappa_n = (4\pi k_B T\lambda)^{-1/2} \exp(-\Delta G^*_{et}/k_B T) \tag{3}$$

where λ and ΔG^*_{et} are the sum of intramolecular reorganization energy λ_{in} and solvent reorganization energy λ_o and Gibbs free energy change of transition state formation, respectively. The reorganization energy is the free energy difference of the product between the minimum energy point and the point corresponding to the minimum energy of the reactant. ΔG^*_{et} was given for the parabolic Gibbs free energies of reactant and product in the high-temperature limit[13,14]

$$\Delta G^*_{et} = (\Delta G^\circ_{et} + \lambda)^2/4\lambda \tag{4}$$

Both ΔG^*_{et} and λ are dependent on temperature in general.

When formation of high-frequency vibrationally excited ($nh\nu$) products is involved in electron-transfer with nuclear displacement of reacting molecules in the inverted region, the nuclear factor of electron transfer from the vibrationally ground state of reactants is written by using Franck−Condon weighted density (FCWD) as following:[15,16]

$$\kappa_n = (4\pi k_B T\lambda)^{-1/2} \exp(-S) \sum_n \exp\left(-\frac{(\Delta G^\circ_{et} + nh\nu + \lambda)^2}{4\lambda k_B T}\right)\frac{S^n}{n!} \tag{5}$$

where S is the electron−vibration coupling coefficient. Because the averaged FCWD over the vibrationally excited states of the

* To whom correspondence should be addressed. E-mail: ohno@ch.wani.osaka-u.ac.jp.

10.1021/jp021257h CCC: $22.00
Published on Web 10/26/2002

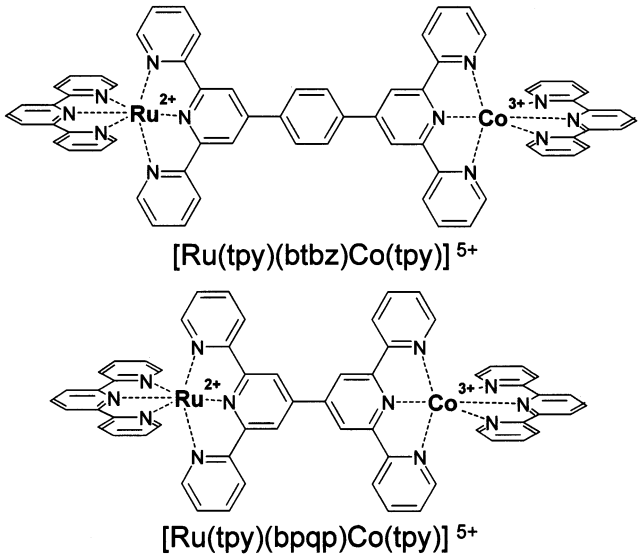

Figure 1. Molecular structures of $[Ru(tpy)(btbz)Co(tpy)]^{5+}$ and $[Ru(tpy)(bpqp)Co(tpy)]^{5+}$.

reactants exhibits a weak and complex temperature-dependence compared with the probability for the classical barrier crossing,[1] the reorganization energy is difficult to assess from the temperature dependence. When the frequencies of low-frequency vibration are changed in such an electron transfer as eq 2,[17,18] the temperature dependence of FCWD makes the evaluation of the reorganization energy more difficult in the inverted region.

Recently, a quantum chemical calculation based on a density functional theory, DFT, has offered optimized structures for both organic compounds and transition metal compounds.[19,20] The quantum chemical calculation has been developed to give not only the frequency of the harmonic vibration in large-size molecules but also the molecular structure of the transition-state.[21,22] The intramolecular reorganization energy based on the molecular structure optimized of the electron transfer product could be compared with that empirically determined.

Reorganization energies for electron-transfer reactions in the normal region were evaluated to be fairly large (2.2−2.3 eV) from the temperature-dependent rate of electron-transfer reaction, $^4Co(II) \rightarrow {}^1Co(III) + e$, in a wide range of temperatures for $[(bpy)_2Ru(BL)Co(bpy)_2]^{5+}$ (BL:2.6-bis(2-pyridyl)benzodiimidazole and 2,2′-bis(2-pyridyl) bibenzimidazole).[23] The rates of intramolecular electron-transfer from the Co(II) moiety to Ru(III) were reduced to $10^7 \sim 10^8\ s^{-1}$ by the large reorganization energy irrespective of a moderate electronic matrix element ($H_{Ru-Co} = 0.8$ meV).[23] The solvent reorganization λ_s is evaluated roughly by using the two-sphere model (TSM)[24,25] or from the transition energy of the Ru(II)-to-Ru(III) charge-transfer band for $[(bpy)_2Ru(BL)Ru(bpy)_2]^{5+}$ [26,27] (BL: 2.6-bis(2-pyridyl)-benzodiimidazole and 1,2-bis (2,2′-bipyridyl-4′-yl)ethane). Two hexadentate bridging ligands are used for the preparation of novel and rigid donor−acceptor Ru−Co compounds, $[Ru(tpy)(btbz)Co(tpy)](PF_6)_5$(tpy = 2,2′:6′,2″-terpyridine, btbz = 1,4-bis[2,2′:6′,2″-terpyridine-4′- yl]benzene) and $[Ru(tpy)(bpqp)Co(tpy)]\ (PF_6)_5$ (bpqp = 6′,6″-bis(2-pyridyl)-2,2′:4′,4″:2″,2‴-quarter-pyridine). Figure 1 shows the structures of the complexes. The averaged length of metal−ligand bonds is estimated to get short by 9 pm in the electron transfer, $Co(II) \rightarrow Co(III) + e$, as in $[Co^{II}(tpy)_2]^{2+}$ where the electronic configuration of Co(II) is $d_\pi{}^6 d_{\sigma^*}$ with doublet spin multiplicity below 250 K for $[Ru^{III}(tpy)(btbz)Co^{II}(tpy)]^{5+}$ and $[Ru^{III}(tpy)(bpqp)Co^{II}(tpy)]^{5+}$.

Sequential reactions, forward electron-transfer (FET) from an excited ruthenium(II) moiety, and the following rapid return electron transfer (RET) were examined for $[Ru^{II}(tpy)(btbz)Co^{III}(tpy)]^{5+}$ and $[Ru^{II}(tpy)(bpqp)Co^{III}(tpy)]^{5+}$ by using time-resolved absorption spectroscopy in the temperature range of 220−350 K. The magnitude of the intramolecular reorganization energy was assessed for the electron-transfer reaction of the doublet electronic configuration of Co(II) forming the singlet one of Co(III) in a wide range of temperatures. The temperature dependence of the spin equilibrium between the doublet and quartet electronic configurations of Co(II) was also investigated. The magnitude of the intramolecular reorganization energy was also evaluated by using a DFT calculation for an electron-transfer reaction, $[Co^{II}(tpy)_2]^{2+} \rightarrow [Co^{III}(tpy)_2]^{3+} + e$.

Experimental Section

Materials. *[Ru(tpy)(btbz)Co(tpy)](PF$_6$)$_5$·6H$_2$O.* A compound of 1,4-bis[1,5-dioxo-1,5-bis(2-pyridyl)pentane-3-yl]benzene was prepared according to the literature and then converted to 1,4-bis[2,2′:6′,2″-terpyridine-4′-yl]benzene (btbz).[28,29] $[Ru(tpy)(btbz)](PF_6)_3 \cdot 8H_2O$ was prepared from btbz and $Ru(tpy)Cl_3 \cdot H_2O$ by refluxing for 2 h.[30−34]

$Co(tpy)Cl_3 \cdot 4H_2O$ was prepared as follows according to the literature.[35] $Na_3[Co(NO_2)_6]$ (120 mg) in 20 mL of H_2O and tpy (70 mg) in 20 mL of H_2O were mixed, and the solution was refluxed for 1 h. The product of $Co(tpy)(NO_2)_3$ was filtered out. Yield: 60 mg (47%). $Co(tpy)(NO_2)_3$ (30 mg) in HCl solution was boiled on a water bath, and a greenish precipitate was formed. Yield: 21 mg (76%). Anal. Calcd for $C_{20}H_{22}Cl_{12}N_4O_3Ru$: C, 38.28; H, 4.07; N, 8.93. Found: C, 38.26; H, 3.35; N, 8.98.

$[Ru(tpy)(btbz)Co(tpy)](PF_6)_5 \cdot XH_2O$ was prepared from $[Ru(tpy)(btbz)](PF_6)_2$ and $Co(tpy)Cl_3$ as follows. $Ru(tpy)(btbz)(PF_6)_2 \cdot 8H_2O$ (11 mg) and $Co(tpy)Cl_3 \cdot 4H_2O$ (4 mg) in 1:1 ethanol−acetonitrile (60 mL) were refluxed for 5 h. The solvent was evaporated, and then the residue was dissolved in water and an excess amount of NH_4PF_6 was added. The solid product was filtered out and purified through CM Sephadex C-25 column. Yield: 10 mg (56%). Anal. Calcd for $C_{66}H_{58}CoF_{30}N_{12}O_6P_5Ru$: C, 39.63; H, 2.92; N, 8.40. Found: C, 40.00; H, 3.01; N, 8.39.

[Ru(tpy)(bpqp)Co(tpy)](PF$_6$)$_5$. $[Ru(tpy)(bpqp)](PF_6)_2 \cdot 6H_2O$ was prepared as follows. $Ru(tpy)Cl_3$ (55 mg) and $AgCF_3SO_3$ (96 mg) in 1:1 ethanol-acetonitrile (80 mL) were refluxed for 16 h. Precipitates of AgCl were removed from the solution. The solvent was evaporated. 6′,6″-Bis(2-pyridyl)-2,2′:4′,4″:2″,2‴-quarter-pyridine (bpqp) was prepared according to the literature.[36] The *N*,*N*-dimethylformamide (DMF) solution of bpqp (58 mg) was added to the residue dissolved in DMF (50 mL) and then refluxed for 2 h. The solvent was evaporated. The residue was dissolved in water, and then an excess amount of NH_4PF_6 was added. The solid product was filtered out and purified through a CM Sephadex LH-20 column. Yield: 14 mg (10%). Anal. Calcd for $C_{45}H_{43}F_{12}N_9O_6P_2Ru$: C, 45.16; H, 3.62; N, 10.53. Found: C, 3.33; H, 45.38; N, 10.58.

$[Ru(tpy)(bpqp)Co(tpy)](PF_6)_5 \cdot 3H_2O$ was prepared as follows. The solution of $Co(tpy)Cl_3 \cdot 4H_2O$ (4 mg) and $AgCF_3SO_3$ (3 mg) in 1:1 ethanol−acetonitrile (40 mL) was refluxed for 16 h. Precipitated AgCl was removed from the solution. The solvent was evaporated. The residue was dissolved in acetonitrile (20 mL). The solution of $[Ru(tpy)(bpqp)](PF_6)_2$ (11 mg) in acetonitrile (20 mL) was added to that of $Co(tpy)(CF_3SO_3)_3$. After refluxing the solution for 2 h, the solvent was evaporated. The residue was dissolved in water, and then an excess amount of NH_4PF_6 was added. The solid product was filtered out and

purified through a CM Sephadex C-25 column. Yield: 2 mg (12%). Anal. Calcd for $C_{60}H_{48}CoF_{30}N_{12}O_3P_5Ru$: C, 38.54; H, 2.59; N, 8.99. Found: C, 38.24; H, 2.78; N, 9.05.

Compounds of $[Co(tpy)_2]Cl_2$ and [Co(4′-tolyl-2,2′:6′,2″-terpyridine)$_2$]Cl_2 were prepared according to the literature.[37] A compound of $[Ru(tpy)(btbz)Ru(tpy)](PF_6)_4$ was a byproduct of $[Ru(tpy)(btbz)](PF_6)_2$.

Measurement. *Preparation of the Sample Solutions.* Acetonitrile was used as a solvent for the measurement in the region of 297−350 K. Butyronitrile was used as a solvent for the measurement in the region of 170−275 K. The solvents were purified by distillation. The sample solutions were prepared just before the measurements.

Cyclic Voltammetry. Redox potentials of the metal complexes were measured by means of differential-pulse voltammetry using a dc pulse polarograph (Huso, HECS-312B). Voltamograms were recorded by using a platinum disk electrode (diameter 0.5 mm) in a solution of the complex containing 0.05 M tetraethylperchlorate ammonium as a supporting electrolyte.

Absorption and Emission Spectra. Absorption spectra of the compounds were measured by using a Shimadzu spectrophotometer (UV-2500PC). Emission spectra were recorded by using a grating monochromator (Jasco CT25-C) with a photodiode image sensor (Hamamatsu C4351), whose sensitivity of detection was corrected by using a bromine lamp (Ushio JPD 100 V, 500WCS).

Time-resolved Difference Absorption Spectra. Nanosecond and picosecond time-resolved difference absorption spectra were obtained by using the second harmonic (SHG) of a Nd^{3+}:YAG laser (Continuum Surelite I-10, $\lambda_{ex} = 532$ nm) and the SHG of a Mode-lock Nd^{3+}:YAG laser ($\lambda_{ex} = 532$ nm, 10 Hz, Continum PY61C-10) for the excitation, respectively. A white light of a Xe-arc lamp was used for acquisition of absorption spectra of longer-living species than 10 ns.[26] TA in the range of 10 ps to 6 ns was acquired using a white light pulse with a delay of 20−6000 ps for the excitation and was produced by focusing the fundamental oscillation laser light into a flowing H_2O/D_2O (1:1 by volume) solution.[23] The fwhm of instrument response function (IRF) were 4 ns and 20 ps for the nanosecond and the picosecond TA acquisition system, respectively.

Subpicosecond time-resolved difference absorption spectra were taken by using laser pulses with a repetition rate of 200 kHz which were generated by a Ti^{3+}:sapphire laser with an oscillator and a regenerative amplifier (Tsunami and Spitfire, Spectra Physics, Inc.). The amplified laser has characteristics of a 100 fs width and an energy of 0.4 mJ with a wavelength centered at 800 nm. The fundamental beam was frequency-doubled by using a 1 mm β-BBO crystal to obtain a 400 nm pump pulse which was used to excite the sample solutions in a 1 mm quartz cell. The remainder of the fundamental beam was focused into an 8 mm flow cell containing water, to generate a white light continuum. A polarizer was used to attain a linear polarization of the probe light and to rotate the polarization to 54.7° (magic angle) relative to that of the pump beam for excitation. Before passing through the sample, the probe beam was divided into a signal and reference beam by a 3 mm beam splitter inserted at 45°. The typical energy of the pump pulse was 50 μJ/pulse with the diameter of 1 mm at the sample. The signal beam through the sample solution and the reference were detected by using image sensors (Hamamatsu S4805-512) attached to a polychromator (Chromex 250IS). The fwhm of IRF was ca. 300 fs.[38] The temperature of the sample solutions (77−300K) was controlled by the use of a cryostat (Oxford DN1704) and a controller (Oxford ITC4)

TABLE 1: Redox Potentials of the Component Compounds and Gibbs Energy Change of the Return Electron-Transfer Process in Butyronitrile at 297 K

compounds	$E°$ ($Ru^{3+/2+}$)	$E°$ ($Co^{3+/2+}$)	$\Delta G°_{RET}$ ($Ru^{3+}-Co^{2+}$/ $Ru^{2+}-Co^{3+}$)
$[Ru(tpy)(btbz)]^{2+}$	1.24		
$[Co(tpy)_2]^{3+}$		0.25	
$[Ru(tpy)(btbz)Co(tpy)]^{5+}$	1.24	0.25	−0.99[a]
$[Ru(tpy)(bpqp)]^{2+}$	1.26		
$[Ru(tpy)(bpqp)Co(tpy)]^{5+}$	1.26		−0.97[a]
$[Co(bpy)_3]^{3+}$		0.28	

[a] $[^2Ru^{3+}-{}^2Co^{2+}] \rightarrow [Ru^{2+}-Co^{3+}]$.

Calculation of the Intramolecular Reorganization Energy. Density functional theory (DFT) calculations were performed using Amsterdam Density Functional (ADF) program package (version 2000.02).[39−41] The intramolecular reorganization energy in the process, $^{2/4}Co(II) \rightarrow {}^1Co(III) + e$, was evaluated as the difference between the bonding energy of the $^1Co(III)$ state at the geometry of the Frank-Condon state and that at the fully relaxed geometry. Because the evaluation of the reorganization energy requires accurate molecular geometries, the geometry optimization was done with tight criterion in convergence (1×10^{-3} hartree/angstrom in energy gradients) and with a fine integration grid (Interger$>$4.5) using a large basis set (basis set IV in ADF package). In this basis set, triple-ζ Slator-type orbitals (STO) are used for valence orbitals, 1s in hydrogen, 2s and 2p in carbon and nitrogen, 3p, 3d, and 4s in cobalt, and 4p, 4d, and 5s in ruthenium, and double-ζ STOs were used for core orbitals. For each atom, one polarization function was added. In case of ruthenium compounds, the relativistic corrections were made using zero-order regular approximation (ZORA).[42−44] The core orbitals 1s−2p of cobalt and 1s−3d for ruthenium were obtained as solutions of a large-basis all-electron calculation on the isolated atom and kept frozen during SCF calculation of the molecule (Frozen core approximation). Both the local density approximation (LDA) with the parametrization of Vosko, Wilk, and Nusair (VWN)[45] and the generalized gradient approximated (GGA) functions by Becke[46] and Perdew[47] (BP) and Perdew-Wang (PW91)[48] were employed.

Results

1. Redox Potentials. Differencial pulse voltamograms (DPV) for $[Ru(tpy)(btbz)]^{3+/2+}$, $[Ru(tpy)(bpqp)]^{3+/2+}$, and $[Co(tpy)_2]^{3+/2+}$ were obtained at 298 K. The peak potentials of DPV vs SCE are shown as the redox potential in Table 1. For most of the binuclear compounds, $[Ru(BL)Co]^{5+}$, DPV displayed two peaks in the range of 0−1.5 V, from which $E°(Co^{3+/2+})$ and $E°(Ru^{3+/2+})$ are determined, respectively. The magnitudes of $\Delta G°_{FET}$ and $\Delta G°_{RET}$ are given from the redox potentials and the excitation energy of $^3CT(Ru)$ for $[Ru(tpy)(btbz)Ru(tpy)]^{4+}$.

2. Absorption Spectra of Ru(II), Ru(III), Co(II), and Co(III) Compounds. A broad band of $[Ru(tpy)(btbz)]^{2+}$ with the peak at 480 nm and intense and sharp bands in the ultraviolet region are characteristic of Ru^{2+}-to-btbz CT and the $\pi-\pi^*$ transition of btbz and tpy coordinated to a metal ion, respectively, as is shown in Figure 2. [Co(4′-tolyl-2,2′:6′,2″-terpyridine)$_2$]$^{3+}$ has no intense absorption band in a visible region. The Ru^{2+}-to-btbz CT band and the $\pi-\pi^*$ bands of $[Ru^{II}(tpy)(btbz)Co^{III}(tpy)]^{5+}$ are more intensive than $[Ru(tpy)(btbz)]^{2+}$ as is shown in Figure 3. $[Ru^{II}(tpy)(bpqp)Co^{III}(tpy)]^{4+}$ exhibits more distinct spectral features, a lower energy shift, and a higher intensity of a Ru^{2+}-to-bpqp CT band compared with $[Ru(tpy)(bpqp)]^{2+}$. The larger transition intensities (larger transition

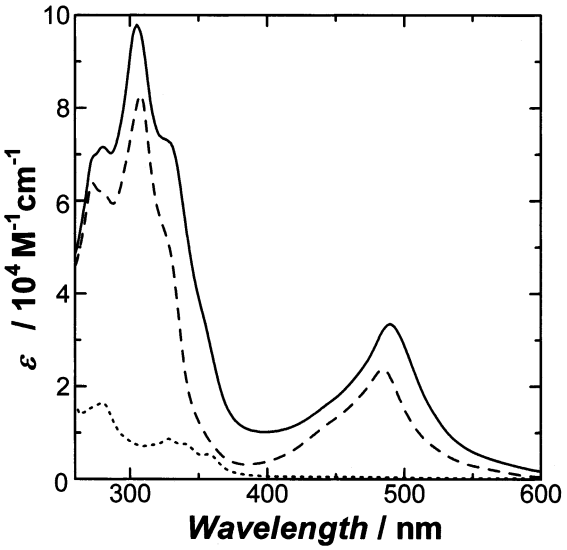

Figure 2. Absorption spectra of $[Ru(tpy)(btbz)]^{2+}$ (dashed line), $[Co(tpy)_2]^{3+}$ (dotted line), and $[Ru(tpy)(btbz)Co(tpy)]^{5+}$ (solid line).

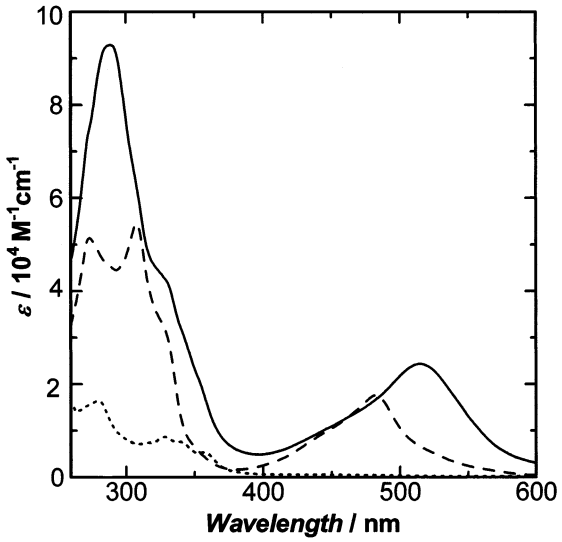

Figure 3. Absorption spectra of $[Ru(tpy)(bpqp)]^{2+}$ (dashed line), $[Co(tpy)_2]^{3+}$ (dotted line), and $[Ru(tpy)(bpqp)Co(tpy)]^{5+}$ (solid line).

dipoles) of MLCT bands are provided by an extended HOMO orbital through the whole ligand on the coordination of btbz and bpqp to Co(III), suggesting more electronic interaction between tpy moieties of btbz and bpqp. The electrochemically oxidized species, $[Ru^{III}(tpy)(bpqp)]^{3+}$ and $[Ru^{III}(tpy)(btbz)]^{3+}$, exhibited a broad and weak band of absorption in the red region and an intense ligand $\pi-\pi^*$ band with blue shifted peaks in the ultraviolet region as is shown in Figure 4. The broad MLCT band of $[Ru(bpqp)(tpy)]^{2+}$ in a visible region appeared in a few minutes because of the reduction of $[Ru(bpqp)(tpy)]^{3+}$.

$[Co(4'\text{-tolyl-}2,2':6',2''\text{-terpyridine})_2]^{2+}$ exhibits five medium-intensity peaks with a spacing of $\sim$1300 cm^{-1} in the 420−600 nm region. The intensity of the band peaks increase with a decrease in temperature in the range of 232 K−312 K as shown in Figure 5, suggesting that the doublet electronic configuration is more predominant at lower temperatures. A composite of the absorption spectra of $[Ru^{III}(tpy)(btbz)]^{3+}$ and $[Co(4'\text{-tolyl-}2,2':6',2''\text{-terpyridine})_2]^{2+}$ is shown in Figure 6.

3. Time-Resolved Difference Absorption Spectra. As Figure 7a shows, a time-resolved difference-absorption spectrum just after the femtosecond laser excitation of $[Ru(tpy)(btbz)Co(tpy)]^{5+}$ consists of a negative and intense band between 400 and 530 nm and a positive and broad band in the longer wavelength region than 530 nm. The difference absorption spectrum resembles those observed on the photoexcitation of $[Ru(tpy)(btbz)]^{2+}$ and $[Ru(tpy)(btbz)Ru(tpy)]^{4+}$ to the $^3CT(Ru)$; the Ru(II)-to-ligand charge transfer (MLCT) absorptions in the 430−530 nm region are bleached, and a weak and broad $\pi-\pi$ transition of a ligand radical and/or ligand-to-Ru(III) (LMCT) charge-transfer transition appears in the region of 530−700 nm. A null difference absorption at 530 nm indicates that the absorption spectrum of $^3CT(Ru)$ has an isosbestic point with that of the ground state. During the following several picoseconds, the difference-absorption in the range of 520−570 nm was reduced to be negative or null. A shift of the null difference absorption point from 530 to 570 nm is characteristic of the conversion of $^3CT(Ru)$ to the second intermediate, which disappeared to regenerate the ground state of $[Ru(tpy)(btbz)Co(tpy)]^{5+}$ in 1 ns as is shown in Figure 7b. The new null difference absorption point indicates that the absorption spectra

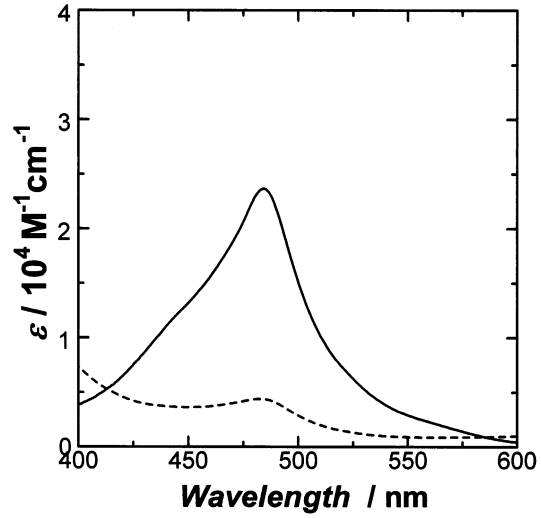

Figure 4. Absorption spectra of $[Ru(tpy)(btbz)]^{2+}$ (dashed line) and $[Ru(tpy)(btbz)]^{3+}$ (broken line).

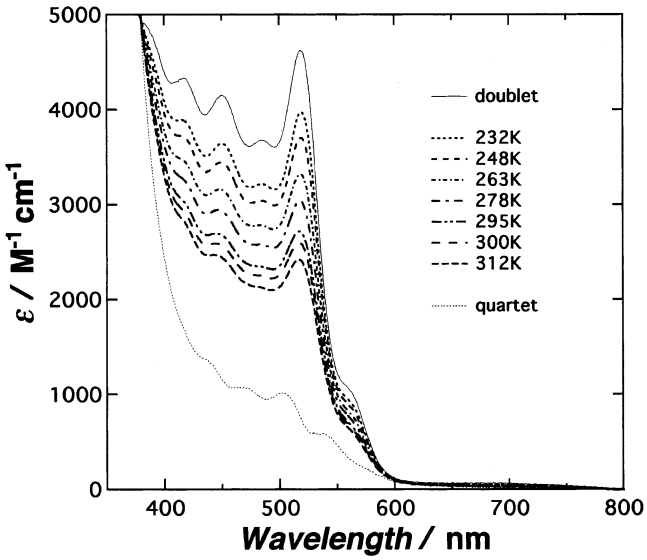

Figure 5. Absorption spectra of $[Co(4'\text{-tolyl-}2,2':6',2''\text{-terpyridine})_2]^{2+}$ at various temperatures. The thin solid line and the thin dotted line stand for the absorption spectra of the doublet electronic configuration and the quartet electronic configuration, respectively.

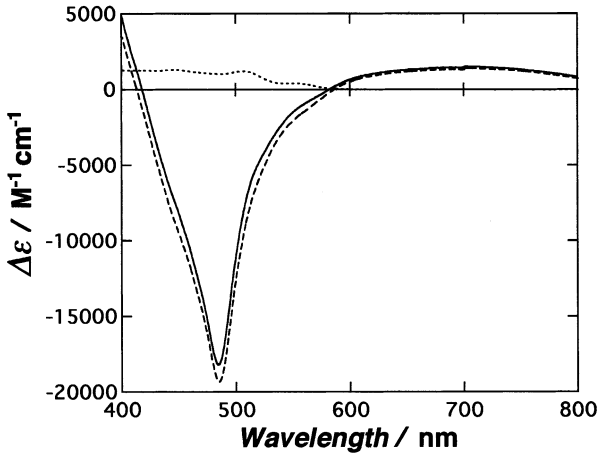

Figure 6. Change of the absorption spectra on the formation of [Ru(tpy)(btbz)]$^{3+}$ (dashed line) and [Co(4′-tolyl-2,2′:6′,2″-terpyridine)$_2$]$^{2+}$ (dotted line). The solid line stands for the sum of the spectral changes.

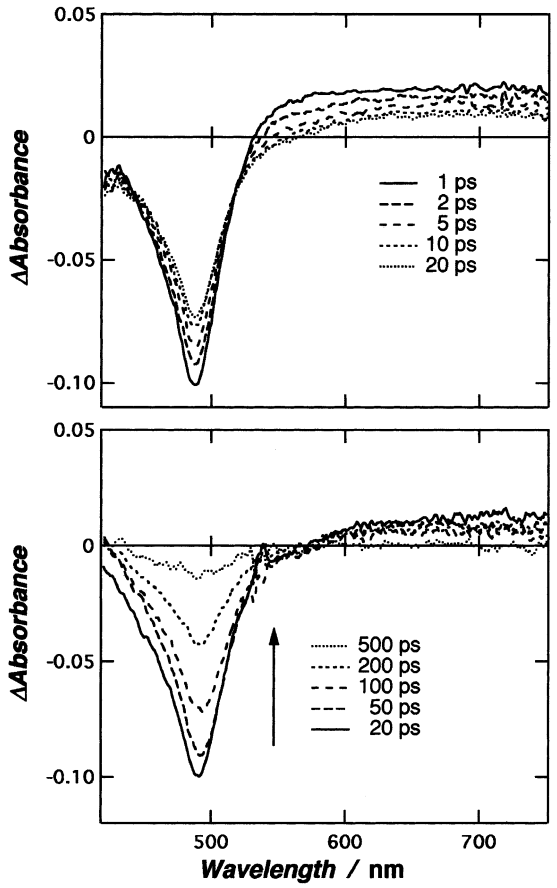

Figure 7. Time-resolved difference absorption spectra of [Ru(tpy)(btbz)Co(tpy)]$^{5+}$ on the laser excitation. The spectra at 1−20 ps after the femtosecond laser excitation and the spectra at 20−500 ps after the picosecond laser excitation are shown in parts a and b, respectively.

of the second intermediate has an isosbestic point with that of the ground state at 570 nm.

As Figure 8 shows, a time-resolved difference-absorption spectrum of [Ru(tpy)(bpqp)Co(tpy)]$^{5+}$ consist of a negative and intense band in the 440−530 nm region and a weakly positive band in the 530−700 nm region just after the femtosecond laser excitation. A similar difference-absorption spectrum was observed for several tens of nanoseconds on the laser excitation of [Ru(tpy)(bpqp)]$^{2+}$. The difference-absorption spectrum was in several picoseconds changed to the second one; the null

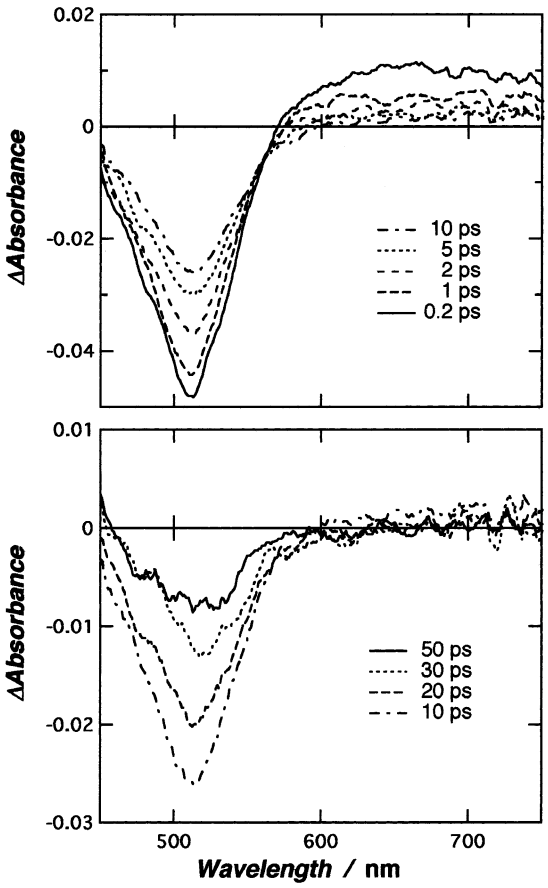

Figure 8. Time-resolved difference absorption spectra of [Ru(tpy)(bpqp)Co(tpy)]$^{5+}$ on the femtosecond laser excitation. The spectra at 0.2−10 ps and at 10−50 ps after the laser excitation are shown in the top figure and the bottom figure, respectively.

difference-absorption was shifted from 530 to 630 nm. In the following time, the intensity of the second difference-absorption spectrum was slowly reduced to null.

4. Time-profile of Difference Absorbance. A laser kinetic spectroscopy revealed that the difference-absorbance at 480 nm on the 400 nm excitation of [Ru(tpy)(btbz)Co(tpy)]$^{5+}$ was changed in two steps as is shown in Figure 9 parts a and b. The first step of the absorption change for 20 ps was detected using a femtosecond laser. The initial absorbance of a positive and broad band around 570 nm disappeared in 10 ps with a rate constant of 0.3×10^{12} s^{-1} for [Ru(tpy)(btbz)Co(tpy)]$^{5+}$, whereas both the negative difference absorbance around 490 nm and the positive band at longer wavelengths than 600 nm remained. A picosecond laser kinetic spectroscopy revealed that the difference-absorption in the whole wavelength range decayed monoexponentially in several nanoseconds. In the second stage of the absorption change, the ground-state absorption (MLCT band) was recovered and the difference-absorbance at 650 nm completely disappeared. The recovery of the MLCT band in the second stage is fitted to the following equation, $\Delta A(t) = \Delta A'_{\mathrm{RET}} \exp(-k_{\mathrm{RET}}'t) + \Delta A_{\mathrm{RET}} \exp(-k_{\mathrm{RET}}t)$, with rate constants k_{RET}' and k_{RET} of 5.6×10^{10} and 0.45×10^{10} s^{-1} at 300 K, respectively, though the fraction $\Delta A_{\mathrm{RET}}'$ was smaller than 0.2 and decreased with increase in the temperature. The apparent rate constant of RET decreased with an increase in temperature from 0.63×10^{10} s^{-1} at 297 K to 1.2×10^{10} s^{-1} at 221 K in butyronitrile and from 0.45×10^{10} s^{-1} at 300 K to 0.68×10^{10} s^{-1} at 233 K in acetonitrile.

The negative difference-absorption at 500 nm produced on the femtosecond laser excitation of [Ru(tpy)(bpqp)Co(tpy)]$^{5+}$

TABLE 2: Phosphoresence Peaks at 77 K, the Decay Rate Constants of ^{3}CT(Ru) (k_{12}) at 297 K, and the Fractions and Rate Constants of Fast ($\Delta A'_{RET}$ and k'_{RET}) and Slow (ΔA_{RET} and k_{RET}) Components of the MLCT Absorption Recovery at 298 K

compounds	$\bar{\nu}^{phos}_{max}$/cm^{-1}	k_{12}/ s^{-1}	$\Delta A'_{RET}$	k'_{RET}/10^9 s^{-1}	ΔA_{RET}	k_{RET}/ 10^9 s^{-1}
[Ru(tpy)(btbz)]$^{2+}$	15 600	8.3×10^8				
[Ru(tpy)(btbz)Ru(tpy)]$^{4+}$	15 500	3×10^8				
[Ru(tpy)(btbz)Co(tpy)]$^{5+}$		3×10^{11}	0.2	56	1	4.5
[Ru(tpy)(bpqp)]$^{2+}$	15 000	2×10^8				
[Ru(tpy)(bpqp)Ru(tpy)]$^{4+}$	14 900	2.3×10^6				
[Ru(tpy)(bpqp)Co(tpy)]$^{5+}$		1×10^{12}	0.08	76	1	30

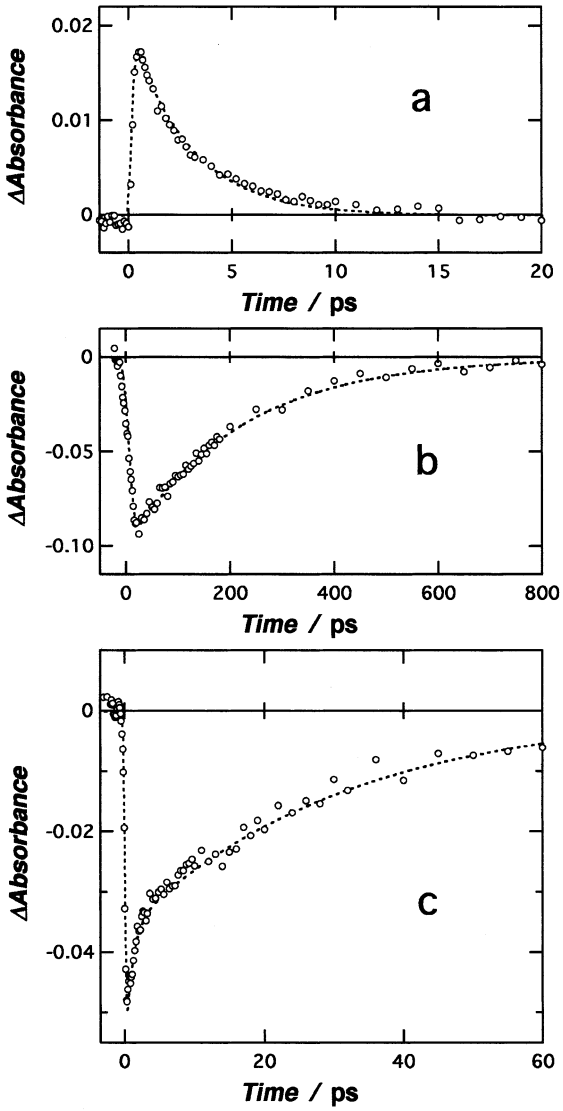

Figure 9. Time profiles of the difference absorption of [Ru(tpy)(btbz)-Co(tpy)]$^{5+}$ (a and b) and [Ru(tpy)(bpqp)Co(tpy)]$^{5+}$ (c) in butyronitrile at 298 K. (a) Decay of a difference absorption at 560 nm with a rate constant of 0.3×10^{12} s^{-1}, and (b) recovery of a difference absorption at 490 nm with a rate constant of 6.3×10^9 s^{-1}. (c) Two-phasic decay of a difference absorption at 510 nm with the rate constants of 1.0×10^{12} and 3.0×10^9 s^{-1} for the fast and the slow decays, respectively. The dashed lines are calculated by using the rate constant(s) of either decay or recovery of difference absorption and the fwhm of IRF.

disappeared biexponentially. The rate constants of the difference-absorption change were 1×10^{12} s^{-1} for the first step and 3.0×10^{10} s^{-1} for the second step at 297 K as is shown in Figure 9c. The rate constants of the first and the second steps are almost independent of the temperature in the temperature range of 282−346 K as Table 3 shows. That of k_{FET} decreased with increase in temperature, whereas that of k_{RET} increased with increase in temperature.

TABLE 3: Rate Constant of the Decay (k_{12}) of ^{3}CT(Ru), the Recovery of Ru(II)−Co(III) (k_{RET}), and the Electron Transfer (k_{20}) from Co(II) of a Doublet Electronic Configuration to Ru(III)

[(tpy)Ru(btbz)Co(tpy)]$^{5+}$

butyronitrile				acetonitrile		
T/ K	k_{12}/ 10^{12} s^{-1}	k_{RET}/ 10^9 s^{-1}	k_{20}/ 10^9 s^{-1}	T/ K	k_{RET}/ 10^9 s^{-1}	k_{20}/ 10^9 s^{-1}
				347	4.8	16
				336	5.2	16
				318	5.5	14
				310	5.5	13
297	0.3	6.3	12	300	4.5	9.4
272		7.3	12	283	5.2	8.0
251		9.0	12	253	5.4	7.4
221		12.0	14	233	6.8	8.2
200		17	19			

[(tpy)Ru(bpqp)Co(tpy)]$^{5+}$

butyronitrile				acetonitrile		
T/ K	k_{12}/ 10^{12} s^{-1}	k_{RET}/ 10^9 s^{-1}	k_{20}/ 10^9 s^{-1}	T/ K	k_{RET}/ 10^9 s^{-1}	k_{20}/ 10^9 s^{-1}
				346	27	91
				333	28	81
				321	29	75
				310	29	67
297	1	30	61	282	31	54
268		33	52			
238		36	45			
213		38	42			
185		38	39			
173		40	41			

Discussion

1. Equilibrium between the Doublet Electronic Configuration and the Quartet Electronic Configuration of [Co(tpy)-(btbz)]$^{2+}$ and [Co(tpy)(bpqp)]$^{2+}$. The electronic configuration and spin multiplicity of most hexacoordinated cobalt(II) compounds are dependent on the coordination structure of ligands. On the symmetrical coordination of the ligands, the electronic configuration of the ground state is $d_{\pi}{}^5 d_{\sigma^*}{}^2$ with a quartet spin multiplicity. The longer bond distances of axial coordinating ligands change the d-orbital configuration of ground state to $d_{\pi}{}^6 d_{\sigma^*}$ with a doublet spin multiplicity. As for [Co(tpy)$_2$]I$_2$·nH$_2$O in a crystalline state,[49,50] and in an aqueous solution,[51] the predominance of doublet electronic configuration was verified by detection of low magnetic susceptivility and high extinction coefficient of a structured absorption band in a visible region. The intensities of structured absorption bands of [Co(4′-tolyl-2,2′:6′,2″-terpyridine)$_2$]$^{2+}$ are dependent on the temperature in a range of 232−312 K as is shown in Figure 7. The stronger absorption intensities at low temperatures are attributable to the greater formation of the doublet electronic configuration. The equilibrium constant between the doublet and the quartet electronic configurations, $K_{23}(T) = C_Q(T)/C_D(T)$, at various

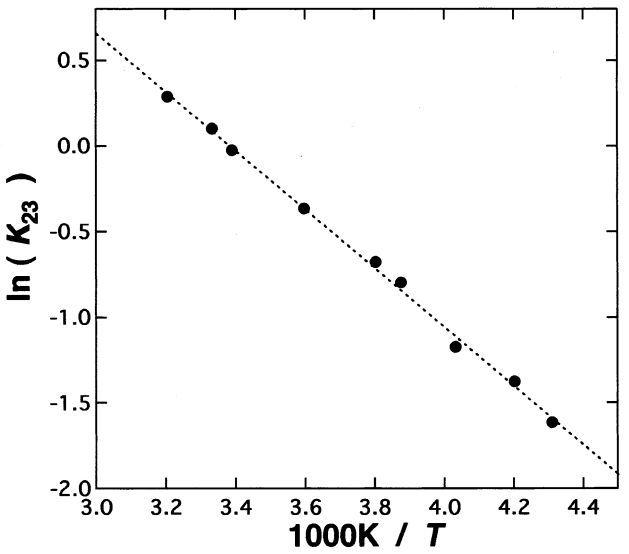

Figure 10. Plot of ln K_{23} verses the reciprocal of temperature for [Co(4′-tolyl-2,2′:6′,2″-terpyridine)$_2$]$^{2+}$.

temperatures were determined by simulating a linear relation between $(K_{23}(T) + 1)\epsilon_{\mathrm{obs},\lambda}$ and $K_{23}(T)$ as follows:

$$(K_{23}(T) + 1)\epsilon_{\mathrm{obs},\lambda} = \epsilon_{\mathrm{D},\lambda} + \epsilon_{\mathrm{Q},\lambda}K_{23}(T) \qquad (6)$$

where $\epsilon_{\mathrm{D},\lambda}$and $\epsilon_{\mathrm{Q},\lambda}$ are the molar extinction coefficients of ^{2}Co(II) and ^{4}Co(II), respectively, and $\epsilon_{\mathrm{obs},\lambda}(T)$ is the mean molar extinction coefficient of Co(II) depending on the temperature. An integrated Gibbs−Helmholz equation of $\ln K_{23}(T) = -\Delta H^\circ_{23}/RT + C$ was satisfied for the temperature-dependent equilibrium constants as is shown in Figure 10 on assuming the temperature-independence of ΔH°_{23}. The quantity of ΔH°_{23} is determined to be 0.148 eV from the linear relation of Gibbs−Helmholz equation, and ΔS°_{23} is 0.50 meV/K from the magnitude of ΔG°_{23} and ΔH°_{23}. The entropy of the quartet-state formation from the doublet state increases as largely as that (0.61 meV/K) of $[Co(tpy)_2]^{2+}$,[23,51] which could be due to both the higher spin multiplicity and the lower frequency of Co−N vibration in the quartet electronic configuration compared with the doublet one.

2. Reaction Scheme and the Changes of Thermodynamic Quantities in the Elementary Processes. The following scheme of reaction, 1∼5, is presumed for photoinduced electron-transfer reactions of [Ru(tpy)(btbz)Co(tpy)]$^{5+}$ and [Ru(tpy)(bpqp)-Co(tpy)]$^{5+}$ (see Figure 11):

(1) process of 0 → 1: photoexcitation of the Ru(II) moiety of Ru(II)-Co(III) to ^{3}CT(Ru)

(2) process of 1 → 2: electron transfer from ^{3}CT(Ru) to Co(III) forming ^{2}Ru(III)−^{2}Co(II)

(3) process of 2 → 0: return electron transfer from ^{2}Co(II) to ^{2}Ru(III)

(4) process of 2 → 3: intersystem crossing forming ^{2}Ru(III)−^{4}Co(II)

(5) process of 3 → 0: return electron transfer from ^{4}Co(II) to ^{2}Ru(III)

Thermodynamic quantities of the processes shown in Table 4 and Figure 11 are evaluated in the following ways. The

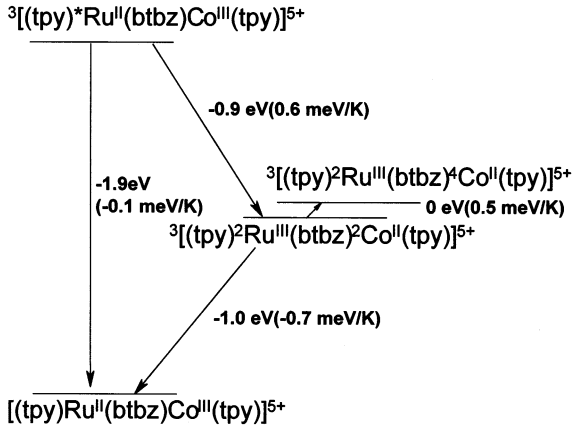

Figure 11. Scheme of photoinduced reaction for [Ru(tpy)(btbz)-Co(tpy)]$^{5+}$.

enthalpy and entropy changes of photoexcitation, ΔH°_{01} and ΔS°_{01}, are taken from the emission peak of the mono-nuclear compound of ruthenium(II) at 77 K and difference in multiplicity between the ground and the excited states. ΔG°_{20} is evaluated to be 0.99 eV from the redox potentials, $E^\circ_{\mathrm{Ru}^{3+/2+}}$ and $E^\circ_{\mathrm{Co}^{3+/2+}}$, of the following half cell reactions, $^2Ru^{3+} + e \rightarrow {}^1Ru^{2+}$ and $^1Co^{3+} + e \rightarrow {}^2Co^{2+}$, respectively. ΔS°_{20} of the return electron-transfer is assumed to be the same (−0.7 meV/K) as that for $[(bpy)_2Ru(BL)Co(bpy)_2]^{5+}$ (BL: 2,2′-bis(2-pyridyl) bibenzimidazole).[23] The large reduction of entropy ΔS°_{20} may arise from an increase in the frequency of Co−N stretching vibration in RET[17,18] and the spin multiplicity change. The increase of entropy (0.6 meV) in the intersystem crossing of the doublet−quartet can be accounted for in terms of the frequency change in the Co−N stretching vibration and the spin multiplicity change.

3. Rates of the Forward Electron Transfer. A difference-absorption spectrum immediately after the laser excitation of [Ru(tpy)(btbz)Co(tpy)]$^{5+}$ is assigned as ^{3}CT(Ru) because of similar (not identical) spectrum to that of $[Ru(tpy)(btbz)]^{2+}$. It was rapidly changed to the second intermediate in an intramolecular process. The spectral change is accounted for by the formation of the ET reaction product, [Ru^{III}(tpy)(btbz)Co^{II}-(tpy)]$^{5+}$, because the difference-absorption spectrum between the second intermediate and the starting compound (Figure 7b) resembles the difference-absorption between the reactant and the products of the following reaction (Figure 6):

$$[^3Ru^{II}(tpy)(btbz)]^{2+} + [Co^{III}(tpy)_2]^{3+} \rightarrow [^2Ru^{III}(tpy)(btbz)]^{3+} + [^2Co^{II}(tpy)_2]^{2+} \qquad (7)$$

The fast decay rate constant of ^{3}CT(Ru), 0.3×10^{12} s^{-1}, is regarded as the rate constant of the forward electron-transfer forming the doublet states of both Ru(III) and Co(II):

$$[^3Ru^{II}(tpy)(btbz)^1Co^{III}(tpy)]^{5+} \rightarrow [^2Ru^{III}(tpy)(btbz)^2Co^{II}(tpy)]^{5+}\, k_{12} \qquad (8)$$

In a similar way, a decay rate constant of ^{3}CT(Ru), 1×10^{12} s^{-1}, is assigned to the forward ET process of [^{3}Ru^{II}(tpy)-(bpqp)^{1}Co^{III}(tpy)]$^{5+}$ based on the time profile of difference-absorption. The removal of the phenylene group from the bridging hexadentate of btbz enhances the overlapping integral between the accepting d_{σ^*} orbital of Co^{2+} and the donating LUMO of btbz, resulting in the faster ET of [^{3}Ru^{II}(tpy)-(bpqp)^{1}Co^{III}(tpy)]$^{5+}$.

TABLE 4: Gibbs Energy Change (ΔG°_{20} and ΔG°_{23}), Entropy Change (ΔS°_{20} and ΔS°_{23}), Activation Energy (E_a), Reorganization Energy (λ_{20} and λ_{30}), and Matrix Element (H_{20} and H_{30}) of RET at 298 K[a]

$Ru^{III}-Co^{II}$	ΔG°_{20}/eV	ΔS°_{20}/meV/K	ΔG°_{23}/eV	ΔS°_{23}/meV/K	E_a/meV	λ_{20}/eV	H_{20}/meV	λ_{30}/eV	H_{30}/meV
$[Ru(tpy)(btbz)Co(tpy)]^{5+}$	−0.99	(−0.70)[b]	0	0.5		0.90	0.8		
$[Ru(tpy)(bpqp)Co(tpy)]^{5+}$	−0.97	(−0.70)[b]	0	0.5		0.85	2.0		
$[Ru(bpy)_2(BL)Co(bpy)_2]^{5+}$ [c]	(−0.98)[d]	(−0.70)[e]	−0.20	0.6	75			2.2	2

[a] The parentheses mean the inferred value. [b] ΔS°_{20} is assumed to be the same as that for $[Ru(bpy)_2$(2,2′-bis(2-pyridyl)bibenzimidazole)$Co(bpy)_2]^{5+}$. [c] BL = 2,2′-bis(2-pyridyl)bibenzimidazole. [d] ΔG°_{20} is the sum of ΔG°_{30} and ΔG°_{23}, the latter of which is assumed to be the same as that of $[Co(bpy)_3]^{2+}$. [e] ΔS°_{20} is the sum of ΔS°_{30} and ΔS°_{23}, the latter of which is assumed to be the same as that for $[Co(tpy)_2]^{2+}$.

4. Rates of Return Electron-Transfer Reactions. The recovery rates of the ground-state absorption of Ru(II) at 297 K (6×10^9 s^{-1} for $[(tpy)Ru^{III}(btbz)Co^{II}(tpy)]^{5+}$ and 3×10^{10} s^{-1} for $[(tpy)Ru^{III}(bpqp)Co^{II}(tpy)]^{5+}$) were determined to be 1/25 and 1/40 of the excited-state quenching rates, respectively. Nonetheless, the recovery rates were much faster than the intramolecular $^4Co^{II}$-to-$^2Ru^{III}$ ET of $[(bpy)(CN)Ru(CN)Co(tpy)(bpy)]^{5+}$ (3×10^9 s^{-1}),[52] $[(bpy)_2Ru^{III}$(2,2′-bis(2-pyridyl)benzodiimidazole)$Co^{II}(bpy)_2]^{5+}$ (2.1×10^8 s^{-1})[23] and 1,2-bis(2,2′-bipyridyl-4′-yl)ethane (1.9×10^7 s^{-1}).[8] The rates measured in this work decreased from 12×10^{10} s^{-1} at 221 K to 6.3×10^{10} s^{-1}at 297 K in butyronitrile. Such an anomalous temperature dependence of the return electron transfer might be partially caused by the decreasing fraction of the doublet electronic configuration of cobalt(II) moiety as the temperature increases, because the doublet electronic configuration of $d_\pi{}^6d_{\sigma^*}$ of $[Co(4'$-tolyl-2,2′:6′,2″-terpyridine$)_2]^{2+}$ in acetonitrile increases its fraction with a decrease in temperature: 0.44 at 312 K to 0.86 at 232 K. On assuming that the RET from the doublet electronic configuration of Co(II) is much faster than that from the quartet electronic configulation, $d_\pi{}^5d_{\sigma^*}{}^2$, the rate constant of RET stemming from ^{2}Co(II), $k_{20}(T)$, is written in terms of the doublet−quartet equilibrium constant, $K_{23}(T)$, which is presumed to be the same for $[(tpy)Ru^{III}(btbz)Co^{II}(tpy)]^{5+}$ and $[(tpy)Ru^{III}(bpqp)Co^{II}(tpy)]^{5+}$ as that of $[Co(4'$-tolyl-2,2′:6′,2″-terpyridine$)_2]^{2+}$:

$$k_{RET}^{obs}(T) = \frac{1}{1 + K_{23}(T)} k_{20}(T) \tag{9}$$

The resulting rate constants $k_{20}(T)$ of $[(tpy)Ru^{III}(btbz)Co^{II}(tpy)]^{5+}$ and $[(tpy)Ru^{III}(bpqp)Co^{II}(tpy)]^{5+}$ in acetonitrile increase from 1.3×10^{10} s^{-1} at 310 K to 1.6×10^{10} s^{-1} at 347 K and from 6.7×10^{10} s^{-1} at 310 K to 9.1×10^{10} s^{-1} at 346 K, respectively. An increase of $k_{20}(T)$ in butyronitrile is smaller as the temperature increases up to 310 K. The rate constant $k_{20}(T)$ of RET in the normal region is semiclassically written in terms of the electronic coupling matrix element, H_{20}, and Gibbs free energy change, $\Delta G^\circ_{20}(T)$:

$$k_{20}(T) = \frac{2\pi}{\hbar} \frac{{H_{20}}^2}{\sqrt{4\pi\lambda_{20}(T)k_BT}} \exp\left[-\frac{(\Delta G^\circ_{20}(T) + \lambda_{20}(T))^2}{4\lambda_{20}(T)k_BT}\right] \tag{10}$$

On taking the temperature-dependence of the Gibbs free energy change and the reorganization energy into account, eq 10 is replaced by the following equation:

$$k_{20}(T) = \frac{2\pi}{\hbar} \frac{{H_{20}}^2}{\sqrt{4\pi\lambda_{20}(T)k_BT}} \exp\left[-\frac{(\Delta H^\circ_{20} - T\Delta S^\circ_{20} + \lambda_{20}(T))^2}{4\lambda_{20}(T)k_BT}\right] \tag{11}$$

where ΔH°_{20} and ΔS°_{20} are the enthalpy change (−0.9 eV) and the entropy change (−0.7 meV/K) in the return electron-transfer, respectively. A weak temperature dependence of $k_{20}(T)$ in Figure 13 is expected for the top region of electron-transfer rate, $-\Delta G^\circ_{20}$ (298 K) = 1 eV ≈ λ_{20}, for which the potential surface of the initial state at the bottom efficiently intersects that of the final state. Two unknown parameters, $\lambda_{20}(T)$ and H_{20}, are evaluated by means of simulation under the assumption of

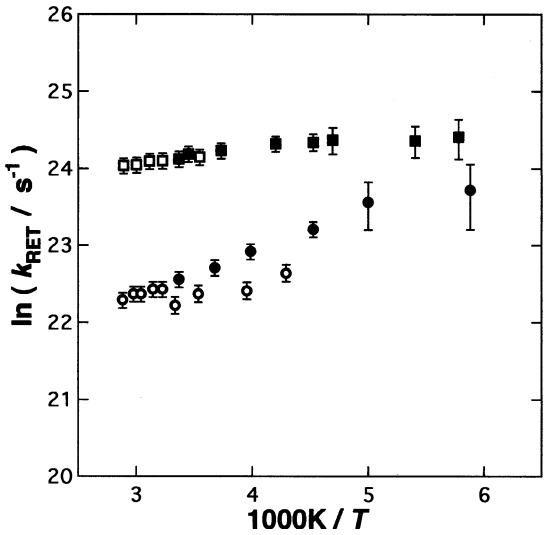

Figure 12. Plots of ln (k_{RET}/s^{-1}) verses $1/T$ for $[Ru(tpy)(btbz)Co(tpy)]^{5+}$ (○ in acetonitrile and ● in butyronitrile) and $[Ru(tpy)(bpqp)Co(tpy)]^{5+}$ (□ in acetonitrile and ■ in butyronitrile) by using different sets of parameters.

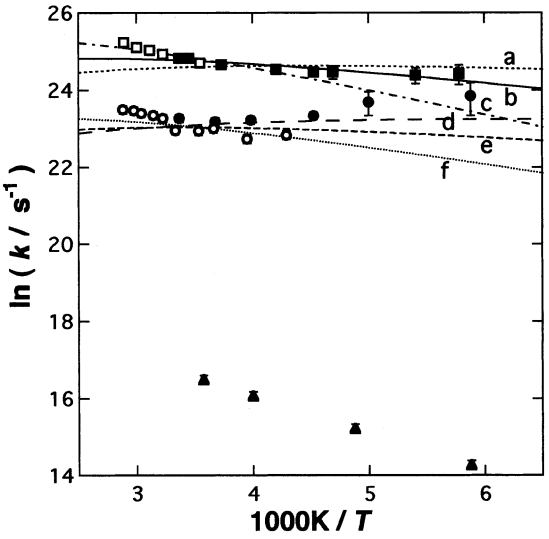

Figure 13. Plots of ln (k_{20}/s^{-1}) verses $1/T$ for $[Ru(tpy)(bpqp)Co(tpy)]^{5+}$ (□ k_{20} in acetonitrile and ■ k_{20} in butyronitrile), $[Ru(tpy)(btbz)Co(tpy)]^{5+}$ (○ k_{20} in acetonitrile and ● k_{20} in butyronitrile), and $[(bpy)_2Ru$(2,2′-bis(2-pyridyl)bibenzimidazole)$Co(bpy)_2]^{5+}$ (▲ k_{40} in butyronitrile[23]). Calculated lines, a−e, are prepared by using ΔH°_{20} of −1.2 eV, ΔS°_2 of 0.7 meV, and a different set of H_{20} and λ_{20} in the following: a, 1.7 meV and 0.95 eV; b, 2 meV and 0.85 eV; c, 2.7 meV and 0.75 eV; d, 0.8 meV and 1.0 eV; e, 0.8 meV and 0.9 eV; f, 0.95 meV and 0.8 eV.

temperature independence of $\lambda_{20}(T)$. The assumption might be reasonable for the solvent reorganization and the intramolecular reorganization, which will be described in the following section. The magnitudes of $\lambda_{20}(T)$ are determined to be 0.90 ± 0.15 and 0.85 ± 0.15 eV for $[(tpy)Ru(btbz)Co(tpy)]^{5+}$ and $[(tpy)Ru(btbz)Co(tpy)]^{5+}$, respectively, from Figure 13 by using ΔS°_{20} of -0.7 meVK^{-1} and ΔH°_{20} of -1.2 eV. The magnitude of ΔS°_{20} is assumed to be the same as that[23] of the redox pair, $[Ru(bpy)_2(2,2'\text{-bis(2-pyridyl)bibenzimidazole})Co(bpy)_2]^{5+}$. The variation of $\Delta G^{\circ}_{20}(T)$ because of the entropy term is 90 meV between 220 and 350 K. The accuracy of λ_{20} in the simulation is considered to be ±0.15 eV on the basis of the differently calculated curves shown in Figure 13. The matrix elements, H_{20}, are also estimated to be 0.8 and 2.0 meV for $[(tpy)Ru(btbz)Co(tpy)]^{5+}$ and $[(tpy)Ru(btbz)Co(tpy)]^{5+}$, respectively, from the temperature dependence of $k_{20}(T)$. They are as small as those (5 and 1 meV) of ^{4}Co(II)-to-^{2}Ru(II) RET in $[Ru^{III}(bpy)_2(BL)Co^{II}(bpy)_2]^{5+}$ (BL: 2,2′-bis(2-pyridyl)-benzodiimidazole)[23] and 1,2-bis(2,2′-bipyridyl-4′-yl)ethane,[8] respectively. The matrix element, H_{12}, for ^{3}CT(Ru)-to-^{1}Co(III) ET in $[(tpy)Ru(btbz)Co(tpy)]^{5+}$ is estimated to be ∼4 meV from the rate (2.5×10^{11} s^{-1}), the Gibbs free energy change (1 eV) and the reorganization energy (0.85 eV) of ET. The role of btbz are different between ET and RET; btbz is the electron donor in ET and the mediator in RET, respectively.

The $k_{20}(T)$'s, 6.1×10^{10} s^{-1}, for $[Ru^{III}(tpy)(bpqp)Co^{II}(tpy)]^{5+}$ and 1.2×10^{10} s^{-1} for $[Ru^{III}(tpy)(btbz)Co^{II}(tpy)]^{5+}$ at 298 K are much larger than the rates of the return electron transfer for $[(bpy)(CN)Ru(CN)Co(tpy)(bpy)]^{5+}$ (0.3×10^{10} s^{-1}),[52] $[Ru^{III}(bpy)_2(2,2'\text{-bis(2-pyridyl)-benzodiimidazole})Co^{II}(bpy)_2]^{5+}$ (0.02×10^{10} s^{-1}),[23] and $[Ru^{III}(bpy)_2(1,2\text{-bis}(2,2'\text{-bipyridyl-4}'\text{-yl})\text{ethane})Co^{II}(bpy)_2]^{5+}$ (0.019×10^{10} s^{-1}).[8] The faster rates of RET in $[^2Ru(BL)^2Co]^{5+}$ (BL: btbz and bpqp) can be attributable to the big difference in the reorganization energy. They are smaller by 1.3 eV than those previously estimated for $[Ru^{III}(bpy)_2(BL)Co^{II}(bpy)_2]^{5+}$ (BL: 2,2′-bis(2-pyridyl)-benzodiimidazole and 2,2′-bis(2-pyridyl)bibenzimidazole).[23] The difference in the reorganization energy is responsible for the difference in the intramolecular reorganization energy as described in the following section.

5. Reorganization Energy of Return Electron Transfer. The reorganization energy of intramolecular ET for $[(L')_2M^{II}_{\alpha}(BL)M^{III}_{\beta}(L'')_2]^{5+}$ can be related to the peak energy (E_{op}) of the lowest-energy M^{II}_{α}-to-M^{III}_{β} charge-transfer (MMCT) band as follows:

$$E_{op} = \Delta G^{\circ}_{MM} + \lambda + 2(H_{II\,III})^2/E_{op} \geq \Delta G^{\circ}_{MM} + \lambda \quad (12)$$

where $H_{II\,III}$ and ΔG°_{MM} are the off-diagonal matrix elements of the $M^{II}_{\alpha}-M^{III}_{\beta}$ interaction related to the intensity of the M^{II}_{α}-to-M^{III}_{β} charge-transfer band and the Gibbs free energy change of a transition from M^{II}_{α}-to-M^{III}_{β} to M^{III}_{α}-to-M^{II}_{β}, respectively. The magnitude of λ is smaller than $E_{op} - \Delta G^{\circ}_{MM}$ by the extent of $2(H_{II,III})^2/E_{op}$, of which the numerator can be estimated from the intensity of MMCT transition. In the case of symmetrical $[L_2Ru^{II}(BL)Ru^{III}L_2]^{5+}$, the lowest energy charge-transfer may arise from the transitions involving nondegenerate dπ orbitals of Ru(II) and appreciably overlap with the second and third lowest-energy bands of charge transfer.[53] The vibrational reorganization λ_{in} is negligibly small for $[LRu^{II}(BL)Ru^{III}L]^{5+}$, though the reorganization energy determined from the optical transition energy of MMCT band can be the sum of vibrational reorganization λ_{in} and the solvent reorganization λ_s. Then the peak energies of the lowest band, 0.96[29] and 0.78 eV[29] for BL = btbz and BL = bpqp in acetonitrile, respectively, could be larger than the solvent reorganization energy by 3% and 8%, respectively, owing to the presence of $Ru^{II}-Ru^{III}$ electronic interaction ($H_{II,III}$). The large widths of the MMCT band suggest the overlapping of higher-energy bands with the lowest one.[29] Consequently, the magnitude of the reorganization enengy is considered to be 90% of the peak energy of MMCT at the maximum. Finally, the solvent reorganization energy is tentatively considered to be 0.85 and 0.70 eV, respectively, for $[(tpy)Ru(BL)Co(tpy)]^{5+}$ (BL = btbz and bpqp) in acetonitrile. The E_{op} of the MMCT band for $[(bpy)_2ClRu^{II}(pyrazine)Ru^{III}Cl(bpy)_2]^{5+}$ and $[(NH_3)_5Ru^{II}(4,4\text{-bpy})Ru^{III}(NH_3)_5]^{5+}$ in water exhibited a weak dependence (-0.25[54] and $+0.12$ meV K^{-1},[55] respectively) on temperature compared with the temperature dependence (0.3 meV K^{-1}) of λ_s estimated below.

The solvent reorganization energy is theoretically estimated by assuming a two-sphere model (TSM).[24,25] TSM assumes that two spheres are surrounded by a hypothetical dielectric continuum of solvent. The solvent reorganization energy is written by using TSM as follows:

$$\lambda_s = \frac{e^2}{4\pi\epsilon_0}\left(\frac{1}{D_o} - \frac{1}{D_s}\right)\left(\frac{1}{2r_D} + \frac{1}{2r_A} - \frac{1}{r_{DA}}\right) \quad (13)$$

where D_o and D_s are the optical and static dielectric constants of solvent, acetonirile (1.8 and 36 at 298 K), or butyronitrile (1.9 and 25 at 298 K), respectively, r_D and r_A are the radius of hypothetical sphere containing a Co^{2+} and a Ru^{3+} at the center, respectively, and r_{DA} is the distance between the point charges on the metal ions. The values of r_D and r_A are smaller than the van der Waals radius (0.6 nm) of the most distant edge of tpy coordinating to a Co^{2+}. The value of r_{DA} is smaller than the center-to-center distance between metal centers, Co^{2+} and Ru^{3+} (1.55 and 1.1 nm for $[Ru(tpy)(btbz)Co(tpy)]^{5+}$ and $[Ru(tpy)(bpqp)Co(tpy)]^{5+}$, respectively), which is estimated to be 85% of the center-to-center distance at least on the quantum chemical calculation of electric dipole moments.[56] The extent of solvent reorganization energy for $[Ru(tpy)(btbz)Co(tpy)]^{5+}$ by presuming r_D, r_A, and r_{DA} as 0.45, 0.45, and 1.3 nm, respectively, is calculated to be 1.1 eV in acetonitrile and 1.0 eV in butyronitrile at 298 K according to eq 13. The extent of solvent reorganization energy for $[Ru(tpy)(bpqp)Co(tpy)]^{5+}$ is estimated to be 0.88 eV in acetonitrile and 0.81 eV in butyronitrile at 298 K by using the following parameters, r_D (0.45 nm), r_A (0.45 nm), and r_{DA} (0.94 nm). TSM affords a large value of λ_s and a weak temperature dependence (0.3 meV K^{-1}) compared with the peak energy of the MMCT band.

The solvent reorganization energies estimated (0.85 and 0.70 eV) are close to those of the total reorganization energies (0.90 ± 0.15 and 0.85 ± 0.15 eV) determined empirically for $[Ru(tpy)(BL)Ru(tpy)]^{5+}$ (BL = btbz and bpqp) in acetonitrile, respectively. Then, the intramolecular reorganization energies of RET for the doublet electronic configuration are estimated to be 0.05 ± 0.15 and 0.15 ± 0.15 eV for $[Ru(tpy)(BL)Ru(tpy)]^{5+}$ (BL= btbz and bpqp) in acetonitrile, respectively. These are much smaller than for the quartet ones ($\lambda_{in} = 2.2-0.85$ eV = 1.4 eV) of $[Ru^{III}(bpy)_2(BL)Co^{II}(bpy)_2]^{5+}$ (BL: 2,2′-bis(2-pyridyl)-benzodiimidazole and 2,2′-bis(2-pyridyl)bibenzimidazole). The big difference might be related to the difference in the molecular structure between the doublet electronic configuration $d_{\pi}{}^6d_{\sigma^*}$ and the quartet electronic configuration $d_{\pi}{}^5\,d_{\sigma^*}{}^2$. The intramolecular reorganization of electron transfer (0−0.3 eV) is considerably smaller than the reorganization energy ($Sh\nu$ = 0.7 eV)[2] of a phosphorescence process for a rhodium(III)

TABLE 5: Optimized Structures of $[Co(bpy)_3]^{3+/2+}$, $[Co(tpy)_2]^{3+/2+}$, and $[Ru(tpy)_2]^{3+/2+}$ and Intramolecular Reorganization Energy (λ_{in}) for $^{2,4}Co(III) \rightarrow Co(II) + e$ and $Ru(II) \rightarrow {}^2Ru(III) + e$

	R(Co−N)/pm, (λ_{in}/eV)	
	$[Co(bpy)_3]^{3+}$	$[^4Co(bpy)_3]^{2+}$
expt	193[a]	213[b]
BP[c]	196	214, (0.87)
PW91[d]	197	214, (0.90)

	R(Co−$N_{central}$, Co−N_{distal})/pm, (λ_{in}/eV)		
	$[Co(tpy)_2]^{3+}$	$[^2Co(tpy)_2]^{2+}$	$[^4Co(tpy)_2]^{2+}$
expt	186, 193[e]	191, 208[f]	203, 214[f]
BP[c]	188, 198	188, 209, (0.27)	204, 215, (0.62)
PW91[d]	188, 197	189, 209, (0.29)	203, 215, (0.68)

	R(Ru−$N_{central}$, Ru−N_{distal})/pm, (λ_{in}/eV)	
	$[Ru(tpy)_2]^{2+}$	$[^2Ru(tpy)_2]^{3+}$
expt	198, 207[g]	
BP[c]	199, 209	200, 209, (0.01)

compound ([Rh(ethylendiamine)Cl_2]Cl) in which the electronic configuration of Rh(III) is changed from $d_\pi{}^5 d_{\sigma^*}$ to $d_\pi{}^6$.

The extent of intramolecular reorganization energy written in Gibbs free energy depends on the nuclear displacement along with the vibrational coordinate. Even if the entropy of the doublet state, S_D, shifts the Gibbs free energy to the negative by $S_D T$ at arbitrary temperature, the reorganization energy as a difference is independent of temperature in the absence of vibrational anharmonicity. When the intramolecular reorganization energy or the nuclear displacement is so small that the anharmonicity may not appear, the intramolecular reorganization energy is almost independent of the temperature. Intramolecular reorganization energy of an ET process can be calculated from an energy difference between the fully relaxed state and the Franck−Condon state of Ru(II)−Co(III), the latter of which retains the same molecular structure as the Ru(III)−Co(II). The potential energies of electronic ground states of Co(II) and Co(III) were evaluated by means of DFT without assuming a harmonic potential surface.[10] The DFT calculation gives rise to the optimized structures of $^2[Co(tpy)_2]^{2+}$ and $^1[Co(tpy)_2]^{3+}$ as are shown in Table 5, each of which is very close to the molecular structure determined by X-ray analysis. The DFT quantum chemical calculation offered the optimized structures of $[Co(bpy)_3]^{3+/2+}$ which are exactly identical to the X-ray structures for $^4[Co(bpy)_3]^{2+}$ and $^1[Co(bpy)_3]^{3+}$, too. The largest error of the ADF calculation is only 4 pm.

The shift of Co−N bond length is calculated to be 12 pm on the average in the ET of $[^2Co^{II}(tpy)_2]^{2+} \rightarrow [^1Co^{III}(tpy)_2]^{3+}$, which is less than half of the bond-length shift (20 pm) for $[^4Co^{II}(tpy)_2]^{2+} \rightarrow [^1Co^{III}(tpy)_2]^{3+}$. The calculated intramolecular reorganization energy of $^2Co^{II} \rightarrow {}^1Co^{III}$ was almost independent of GGA functions (BP or PW91) and was 0.27−0.29 eV for the doublet electronic configuration. Meanwhile, the reorganization energies are estimated to be 0.65 and 0.9 eV for $^4Co^{II}-{}^2Ru^{III} \rightarrow {}^1Co^{III}-Ru^{II}$ in $[Co(tpy)_2]^{2+/3+}$ and $[Co(bpy)_3]^{2+/3+}$, respectively, assuming that intramolecular reorganization energy of Ru(III)/Ru(II) redox process is the same as that for $[Ru(tpy)_2]^{3+/2+}$. The calculated values of intramolecular reorganization energy (0.27−0.29 and 0.9 eV) are in a good agreement with those (0−0.3 and 1.3 eV) empirically determined above for RET of $[Ru(tpy)(bpqp)Ru(tpy)]^{5+}$ and [Ru(bpy)$_2$(2,2′-bis(2-pyridyl)bibenzimidazole)Co(bpy)$_2$]$^{5+}$, respectively.

6. Intersystem Crossing (ISC) between ^{2}Co(II) and ^{4}Co(II). An attempt was made to detect the doublet−quartet ISC process after the formation of ^{2}Co(II). The ISC could be detected, provided that the ISC rate is slower than the FET and faster than the RET. The absorption change with the ISC at 500 nm ($\Delta\epsilon_{D\rightarrow Q} = -3500\ M^{-1}\ cm^{-1}$ for $[Co(btbz)_2]^{2+}$) was, however, small compared with the recovery of the ground-state molecule ($-29\,000\ M^{-1}cm^{-1}$) of the ET product. Therefore, the ISC process could not be separated from the absorption change because of the fast RET of $[Ru(tpy)(btbz)Co(tpy)]^{5+}$ and $[Ru(tpy)(bpqp)Co(tpy)]^{5+}$.

If the RET of the doublet electronic configuration is fast enough to compete with the ISC to the quartet one (eq 6), the recovery of the ground-state absorption occurs biexponentially. The doublet electronic configuration undergoes RET (eq 15) in a competition with the ISC process (eq 14) in an early time. Then it does in a later time after an equilibration between the doublet and quartet electronic configurations (eqs 14 and 16) has been established:

$$[^2Ru^{III}(bpy)_2(btbz)^2Co^{II}(bpy)_2]^{5+} \rightarrow [^2Ru^{III}(tpy)(btbz)^4Co^{II}(tpy)]^{5+}\ k_{23} \quad (14)$$

$$[^2Ru^{III}(tpy)(btbz)^2Co^{II}(tpy)]^{5+} \rightarrow [Ru^{II}(tpy)(btbz)Co^{III}(tpy)]^{5+}\ k_{20} \quad (15)$$

$$[^2Ru^{III}(bpy)_2(btbz)^4Co^{II}(bpy)_2]^{5+} \rightarrow [^2Ru^{III}(tpy)(btbz)^2Co^{II}(tpy)]^{5+}\ k_{32} \quad (16)$$

$$[^2Ru^{III}(tpy)(btbz)^4Co^{II}(tpy)]^{5+} \rightarrow [Ru^{II}(tpy)(btbz)Co^{III}(tpy)]^{5+}\ k_{30} \le k_{20} \quad (17)$$

A biexponential recovery of the ground-state absorption for $[Ru(tpy)(btbz)Co(tpy)]^{5+}$ was observed at low temperatures, where the fraction of the fast decay component was 20% at the largest. As for $[Ru(tpy)(bpqp)Co(tpy)]^{5+}$, the recovery of the ground-state absorption was fast ($3 \times 10^{10}\ s^{-1}$) and single exponential at all temperatures. Hence, the ISC in $[Ru(tpy)(BL)Co(tpy)]^{5+}$ is considered to be much faster than RET ($3 \times 10^{10}\ s^{-1}$) even at low temperatures.

Conclusion

A study of laser kinetic spectroscopy on $[Ru^{II}(tpy)(btbz)Co^{III}(tpy)]^{5+}$ and $[Ru^{II}(tpy)(bpqp)Co^{III}(tpy)]^{5+}$ revealed that there is a rise-and-decay of two transient species, ^{3}CT(Ru) and the electron-transfer product of $[Ru^{III}(BL)Co^{II}]^{5+}$ for 1 ns. ^{3}CT(Ru) decayed with a rate constant of more than $10^{11}\ s^{-1}$ to produce the intramolecular electron-transfer product of $[Ru(III)(BL)Co(II)]^{5+}$. The intramolecular ET product of $[Ru^{III}(BL)Co^{II}]^{5+}$ with a doublet electronic configuration $d_\pi{}^6 d_{\sigma^*}$ of Co(II) was converted to the reactant of $[Ru^{II}(BL)Co^{III}]^{5+}$ (BL:btbz and bpqp) with a 50 times larger rate constant ($(1\sim3) \times 10^{10}\ s^{-1}$) than those of $[Ru^{III}(BL)Co^{II}]^{5+}$ (BL: 2.6-bis(2-pyridyl)benzodiimidazole and 2,2′-bis(2-pyridyl) bibenzimidazole) with a quartet electronic configuration $d_\pi{}^5\, d_{\sigma^*}{}^2$ of Co(II).[23] The reorganization energy (0.95 ± 0.15 eV) was determined on the basis of the weakly temperature-dependent RET rate by taking the negative entropy change (-0.7 meV/K) of the RET process and the closely lying quartet state into consideration. Both the small reorganization energy and the moderate electronic coupling matrix element (0.8 and 2 meV) for $[Ru^{II}(tpy)(btbz)Co^{III}(tpy)]^{5+}$ and $[Ru^{II}(tpy)(bpqp)Co^{III}(tpy)]^{5+}$ are responsible for the larger rates of the RET compared with $[Ru^{III}(BL)Co^{II}]^{5+}$ (BL: 2.6-bis(2-pyridyl)benzodiimidazole and 2,2′-bis(2-pyridyl) biben-

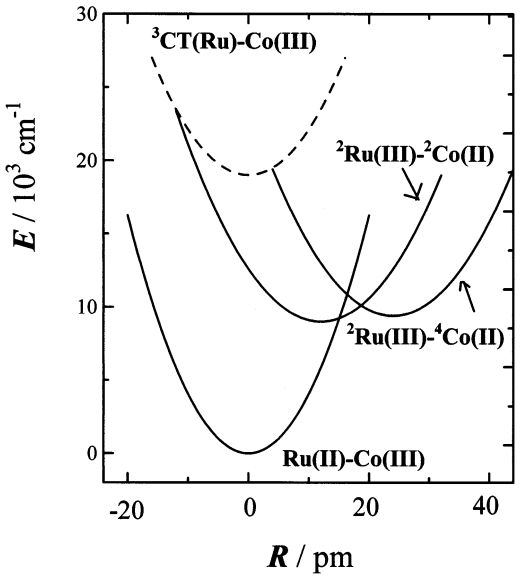

Figure 14. Schematic potential curves of the ground state, the ^{3}CT-(Ru), [Ru(tpy)(btbz)^{2}Co(tpy)]$^{5+}$, and [Ru(tpy)(btbz)^{4}Co(tpy)]$^{5+}$ involved in ET and RET of [Ru(tpy)(btbz)Co(tpy)]$^{5+}$.

zimidazole). Solvent reorganization energies of RET in [Ru^{II}-(tpy)(btbz)Co^{III}(tpy)]$^{5+}$ were empirically estimated to be 0.85 eV in acetonitrile and 0.78 eV in butyronitrile from the MMCT transition energy of [Ru^{II}(tpy)(btbz)Ru^{III}(tpy)]$^{5+}$.[29] The residues of reorganization energies (0−0.3 eV) are ascribed to the intramolecular reorganization of the return electron transfer in [Ru^{II}(tpy)(btbz)Co^{III}(tpy)]$^{5+}$ and [Ru^{II}(tpy)(bpqp)Co^{III}(tpy)]$^{5+}$, respectively. The intramolecular reorganization energies of the ^{2}Co(II)/^{1}Co(III) redox are much smaller than those estimated for ^{4}Co(II)/^{1}Co(III).[23] The magnitude of the intramolecular reorganization energy is in agreement with those (0.27−0.29 eV) calculated by using a density functional theory (Figure 14).

Acknowledgment. K.N. gratefully acknowledges financial support from the Ministry of Education, Science, Sports and Culture for a Grant-in-Aid for Scientific Research (No. 12640556 and 13128206).

References and Notes

(1) Bixon, M.; Jortner, J. *J. Phys. Chem.* **1993**, *97*, 13061.
(2) Islam, A.; Ikeda, N.; Nozaki, K.; Ohno, T. *J. Chem. Phys.* **1998**, *109*, 4900.
(3) Schmidt, K. H.; Müller, A. *Inorg. Chem.* **1975**, *14*, 2183.
(4) Endicott, J. F.; Durham, B.; Glick, M. D.; Anderson, T. J.; Kuszaj, J. M.; Schmonsees, W. G.; Balakrishnan, K. P. *J. Am. Chem. Soc.* **1981**, *103*, 1431.
(5) Lewis, N. B.; Coryell, C. D.; Irvine, J. W. *J. Chem. Soc.* **1949**, 5386.
(6) Dwyer, F. P.; Sargeson, A. M. *J. Phys. Chem.* **1961**, *65*, 1892.
(7) Borchardt, D.; Pool, K.; Wherland, S. *Inorg. Chem.* **1982**, *21*, 93.
(8) Endicott, J. F.; Kumar, K.; Ramasami, T.; Rotzinger, F. P. *Prog. Inorg. Chem.* **1983**, *30*, 141.
(9) Buhks, E.; Bixon, M.; Jortner, J.; Navon, G. *Inorg. Chem.* **1979**, *18*, 2014.
(10) Sutin, N. *Prog. Inorg. Chem.* **1983**, *30*, 441.
(11) Newton, M. D. *J. Phys. Chem.* **1991**, *95*, 30.
(12) Ungar, L. W.; Newton, M. D.; Voth, G. A. *J. Phys. Chem. B* **1999**, *99*, 7367.
(13) Marcus, R. A. *J. Chem. Phys.* **1956**, *24*, 966.
(14) Newton, M. D. In *Electron Transfer in Chemistry*; Balzani, V., Ed.; 2001, 1, 1.
(15) Liang, N.; Miller, J. R.; Closs, G. L. *J. Am. Chem. Soc.* **1990**, *112*, 5353.
(16) Chen, P.; Duesing, R.; Graff, D. K.; Meyer, T. J. *J. Phys. Chem.* **1991**, *95*, 5850.
(17) Richardson, D. E.; Sharpe, P. *Inorg. Chem.* **1991**, *30*, 1412.
(18) Crawford, P. W.; Schultz, F. A. *Inorg. Chem.* **1994**, *33*, 4344.
(19) Ziegler, T. *Chem. Rev.* **1991**, *91*, 651.
(20) Wong, M. W. *Chem. Phys. Lett.* **1996**, *256*, 391.
(21) El-Azhary, A. A.; Suter, H. U. *J. Phys. Chem.* **1996**, *100*, 15056.
(22) Scott, A. P.; Radom, L. *J. Phys. Chem.* **1996**, *100*, 16502.
(23) Yoshimura, A.; Nozaki, K.; Ikeda, N.; Ohno, T. *J. Phys. Chem.* **1996**, *100*, 1630.
(24) Marcus, R. A. *Can. J. Chem.* **1959**, *37*, 155.
(25) Marcus, R. A. *J. Chem. Phys.* **1965**, *43*, 2654.
(26) Ohno, T.; Nozaki, K.; Haga, M. *Inorg. Chem.* **1992**, *31*, 548.
(27) Ohno, T.; Nozaki, K.; Haga, M. *Inorg. Chem.* **1992**, *31*, 4256.
(28) Constable, E. C.; Cargill Thompson, A. M. W. *J. Chem. Soc., Dalton Trans.* **1992**, 3467.
(29) Collin, J. P.; Laine, P.; Launay, J. P.; Sauvage, J. P.; Sour, A. *J. Chem. Soc., Chem. Commun.* **1993**, 434.
(30) van Vliet, P. M.; Toekimin, S. M. S.; Haasnoot, J. G.; Reedijk, J.; Nováková, O.; Vrána, O.; Brabec, V. *Inorg. Chim. Acta* **1995**, *231*, 57.
(31) Adcock, P. A.; Keene, F. R.; Smythe, R. S.; Snow, M. R. *Inorg. Chem.* **1984**, *23*, 2336.
(32) Beley, M.; Collin, J. P.; Louis, R.; Metz, B.; Sauvage, J. P. *J. Am. Chem. Soc.* **1991**, *113*, 8521.
(33) Indelli, M. T.; Scandola, F.; Collin, J. P.; Sauvage, J. P.; Sour, A. *Inorg. Chem.* **1996**, *35*, 303.
(34) Barigelletti, F.; Flamigni, L. Calogero, G. Hammarström, L.; Sauvage, J. P.; Collin, J. P. *J. Chem. Soc., Chem. Commun.* **1998**, 2333.
(35) Crayton, P. H. *Inorg. Synth.* **1963**, *7*, 207.
(36) Beley, M.; Chodorowski, S.; Collin, J.-P.; Sauvage, J.-P. *Tetrahedron Lett.* **1993**, *34*, 2933.
(37) Figgis, B. N.; Kucharski, E. S.; White, A. H. *Aust. J. Chem.* **1983**, *36*, 1527.
(38) Tsushima, M.; Motojima, Y.; Ikeda, N.; Yonehara, H.; Etori, H.; Pac, C.; Ohno, T. *J. Phys. Chem. A* **2002**, *106*, 2256.
(39) Baerends, E. J.; Ellis, D. E.; Ros, P. *Chem. Phys*. **1993**, *2*, 42.
(40) Boerrigter, P. M.; Velde, G. te.; Baerends, E. J. *Int. J. Quantum Chem.* **1988**, *33*, 87.
(41) Velde, G. te.; Baerends, *J. Comput. Phys*. **1992**, *99*, 84.
(42) van Lenthe, E.; Baerends, E. J.; Snijders, J. G. *J. Chem. Phys*. **1993**, *99*, 4597; **1994**, *101*, 9783.
(43) van Lenthe, E.; Snijders, J. G.; Baerends, E. J. *J. Chem. Phys*. **1996**, *105*, 6505.
(44) van Lenthe, E.; Ehlers, A.; Baerends, E. J. *J Chem. Phys.* **1999**, *110*, 8943.
(45) Vosko, S. H.; Wilk, L.; Nusair, M. *Can. J. Phys.* **1980**, 5*8*, 1200.
(46) Ehlers, A. E.; Becke, A. D. *Phys. Rev. A* **1988**, *38*, 3098.
(47) Perdew, J. P. *Phys. Rev. B* **1986**, *33*, 8822.
(48) Perdew, J. P.; Chevary, J. A.; Vosko, S. H.; Jackson, K. A.; Pederson, M. R.; Singh, D. J.; Fiolhais, C. *Phys. Rev. B* **1992**, *46*, 6671.
(49) Harris, C. M.; Lockyer, T. N.; Martin, R. L.; Patil, H. R. H.; Sinn, E.; Stewart, I. M. *Aust. J. Chem.* **1969**, *22*, 2105.
(50) Judge, J. S.; Baker, W. A. *Inorg. Chim. Acta* **1967**, *1*, 68.
(51) Binstead, R. A.; Beattie, J. K. *Inorg. Chem.* **1986**, *25*, 1481.
(52) Buranda, T.; Lei, Y.; Endicott, J. F. *J. Am. Chem. Soc.* **1992**, *114*, 6916.
(53) Demadis, K. D.; Hartshorn, C. M.; Meyer, T. J. *Chem. Rev*. **2001**, *101*, 2655.
(54) Hupp, J. T.; Neyhart, G. A.; Meyer, T. J.; Kober, E. M. *J. Phys. Chem.* **1992**, *96*, 10820.
(55) Dong, Y.; Hupp, J. T. *Inorg. Chem.* **1992**, *31*, 3322.
(56) Nelson, S. F.; Newton, M. D. *J. Phys. Chem. A* **2000**, *104*, 10023.